20th IMEKO TC4 International Symposium and
18th International Workshop on ADC Modelling and Testing
Research on Electric and Electronic Measurement for the Economic Upturn
Benevento, Italy, September 15-17, 2014

A Self-Oscillating System to Characterize Liquid Salinities within a Single Triangular Waveform Signal

Laurent A. Francis, Sylvain Druart, and Denis Flandre

Electrical Engineering Department, ICTEAM Institute, Université catholique de Louvain, Place du Levant 3, BE-1348 Louvain-la-Neuve, Belgium
{laurent.francis, sylvain.druart, denis.flandre}@uclouvain.be

***Abstract* – In this paper, we present a methodology and a circuit to extract liquid mixtures resistance and capacitance simultaneously from the same output signal using interdigitated sensing electrodes. The principle is based on the triangular waveform voltage signal generation technique where a current square wave is applied to the sensor and results in a triangular output voltage that contains both the conductivity and permittivity parameters in a single periodic segment. A closed-loop current controlled oscillator that operates on a single DC power supply implements this concept. The system interface is portable and only a small number of electrical components are used to generate the expected signal. As test examples, the electrical conductivities of saline NaCl and KCl solutions are characterized by a system prototype and benchmarked against a commercially available equipment. The results show excellent linearity and prove the repeatability of the measurements.**

I. INTRODUCTION

Quantifying the salinity of liquids is of major interest for fluid identification in several domains like medicine, biology or chemistry. In order to face this complex challenge, instrumentation solutions are constantly developed. In this paper, we are focused on the electrical measurement of liquid mixtures in order to extract their impedance modeled as an R-C parallel dipole [1–3]. In most cases, the sensing device is an impedimetric sensor with interdigitated electrodes (IDE) stimulated by a sinusoidal wave. The fluid impedance is then extracted out of the modulus and the phase of the response. Instead of the sinusoidal waveform, a triangular waveform voltage (TWV) is a more effective stimulation [4,5]. This technique has been used successfully to sense constant phase element impedances but the extraction of the sensed data required to count all the elapsed periods of the triangular signal after its generation [6]. In this paper, the proposed sensor interface implements the TWV approach principle starting from a square current signal for measuring the conductivity and permittivity of liquids modeled as R-C parallel dipoles.

A first improvement consists in isolating each voltage segment into a compact equation independent from the previous states of the oscillating wave. Therefore, the signal analysis is highly simplified and only requires sampling the data of a signal period to get all the expected parameters of a tested liquid.
A second one is the implementation of a current-controlled oscillator (CCO) circuit of simple architecture so that the resulting solution requires a single DC power source to operate. Autonomous systems are indeed highly advantageous to improve the compactness and the portability of sensing systems, in particular for measurement systems with large signal variations such as for example in an other of our work where interdigitated electrodes are used as dew sensor for human breathing [7].

II. SENSING ELEMENT MODEL

The IDE sensor structure is provided in Fig. 1, where V_a and V_b are the electrical contacts. The microelectrodes are made of a conductive material patterned on an insulating board. A cell is defined as the periodic element of the entire IDE structure in order to provide boundaries for the calculation domain of the impedance. We neglect the edge effects and the geometrical parameters are reported in Table 1 while Eq. (1) provides the impedance Z_S for the electrical model (Fig. 2) represented as a global R-C parallel dipole. The components R_L and C_L are linked to, respectively, the fluid conductivity σ_L and permittivity ε_L by the geometrical factor defined in Eq. (2) as the cell constant c_k expressed in m^{-1} [1]. The component C_B is the parasitic substrate capacitance. For the electrodes, gold is preferred as highly cathodic material that allows for neglecting the interface solid-liquid effects. Indeed, the low ionic adsorption on gold reduces the faradaic current transfer [2] and the formation of an electrical double layer (EDL) [1]. The microelectrodes are also considered wide enough in comparison with the typical thickness of the

ISBN-14: 978-92-990073-2-7

EDL to allow for neglecting the impact of double layer capacitance, *i.e.* > 1 µm [8].

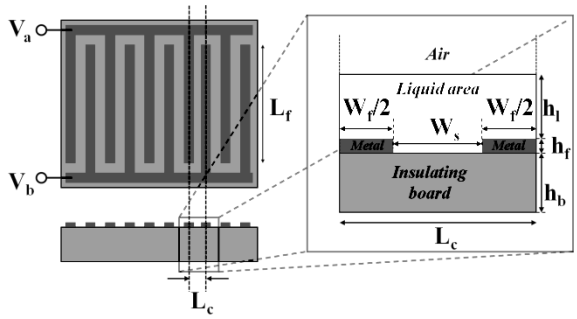

Fig. 1: Schematic global view and cross-section of the interdigitated electrodes (IDE) sensor.

Table 1: Parameter description

Name	Symbol	Units
Tested fluid thickness	h_l	[m]
Board thickness	h_b	[m]
Electrodes height	h_f	[m]
Electrodes width	W_f	[m]
Electrodes spacing	W_s	[m]
Cell width	L_c	[m]
Electrodes length	L_f	[m]
Electrodes number	N_f	[-]

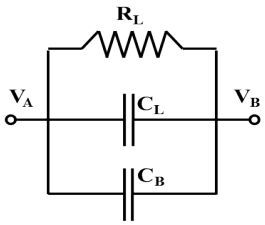

Fig. 2: IDE sensor electrical equivalent model.

$$Z_S = \frac{R_L}{1+sR_L(C_L+C_B)} \qquad (1)$$

$$c_k = \sigma_L R_L = \frac{\varepsilon_L}{C_L} \qquad (2)$$

The impedance values were computed by help of finite elements modeling (FEM) using COMSOL Multiphysics® software. The time-harmonic Laplace is solved over a meshed domain bounded by a cell structure periodic element that gives access to both cell constants in the bulk and in the sensitive area, c_{kB} and c_{kL} given by Eq. (3). The bulk and fluid capacitances and the fluid resistance are given by Eq. (4). FEM has been chosen because the IDE classical analytical formulas given in [9] do not consider the finger height and make the cell constant estimation less accurate.

$$\begin{cases} c_{kL} = \frac{\Delta V}{\int_0^{h_l} E_x dy} \\ c_{kB} = \frac{\Delta V}{\int_{-h_b}^{0} E_x dy} \end{cases} \qquad (3)$$

$$\begin{cases} R_L = \frac{c_{kL}}{\sigma_L N_f L_f} \\ C_L = \frac{\varepsilon_L N_f L_f}{c_{kL}} \\ C_B = \frac{\varepsilon_B N_f L_f}{c_{kB}} \end{cases} \qquad (4)$$

III. SENSOR STIMULATION THEORY

The IDE structure model is included in an electrical circuit with an additional serial capacitance C_S (Fig. 3) needed to generate the triangular shape of the output signal as it cuts the DC path from the analog voltage node to the ground. The circuit loads the device under test with a square current signal *i(t)* and the response voltage $v_a(t)$ is then probed. The total impedance Z_C loaded by the square current is given by the following equation:

$$Z_C = \frac{1}{sC_L} + Z_S \qquad (5)$$

Applying the TWV theory in the case of the impedance $Z_C(s)$, a square-shaped current wave (7) of amplitude I_0 and period 2T stimulates the impedance, *u(t)* being the unit hard-step function. As shown in [6], the two first steps of the current wave have respectively $I_0/2$ and $3I_0/2$ of amplitude to keep mean value of the voltage response at zero.

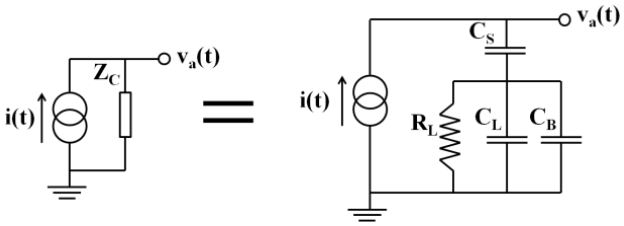

Fig. 3: Impedance Z_C stimulated by a current.

$$i(t) = \frac{I_0}{2}u(t) - \frac{3I_0}{2}u(t-T) + 2I_0\sum_{n=2}^{\infty}(-1)^n u(t-nT) \qquad (6)$$

The application of the inverse Laplace transform on the $Z_C(s)I(s)$ product gives the time domain voltage response wave expression given by Eq. (6), introducing three shaping parameters named in Table 2 as β, ζ and τ . The plots sketched in Fig. 4 illustrate the time progression of the current wave and the voltage output wave for several values of the model electrical components.

Table 2: Voltage response shaping parameters

Symbol	Expression	Units
β	I_0/C_S	[V/s]
ζ	I_0R_L	[V]
τ	$R_L(C_L+C_B)$	[s]

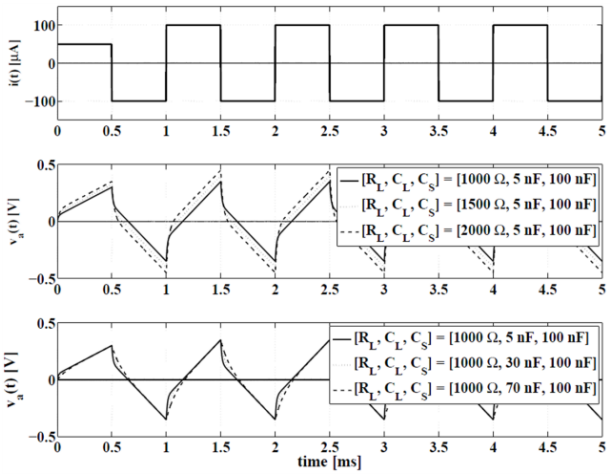

Fig. 4: Transient square current (top wave) and voltage response for resistive component variation (middle wave) and capacitive component variation (bottom wave).

The transient development gave the output voltage wave as a series expression. Each rising or falling wave segment contains all the information we are seeking about the tested impedance. A compact equation of wave segments thus needs to be calculated to extract the curve parameters β, ζ and τ. The curve plotted in Fig. 5 summarizes the parametric representation of a wave segment with the definition of a variable ζ'. The segment wave comprises two distinct parts, an exponential one and a linear one.

$$v_u(t) = \beta t + \frac{2\zeta}{1+e^{\left(-\frac{T}{\tau}\right)}}\left(1 - e^{\left(-\frac{t}{\tau}\right)}\right) \qquad (7)$$

$$\zeta' = \frac{2\zeta}{1+e^{\left(-\frac{T}{\tau}\right)}} \qquad (8)$$

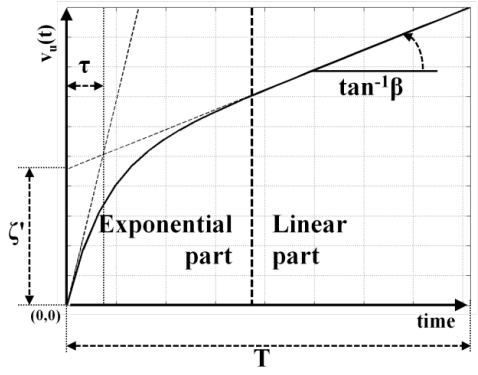

Fig. 5: Output voltage wave segment shape.

Equation (7) is the compact mathematical form of each wave segment. Three particular cases can be observed from this expression.

The first case is when the exponential part of $v_u(t)$ is predominant, which appears when the time constant τ is greater than the current wave oscillation half-period ($\tau >> T$). The top curves of Fig. 6 illustrate how this first case is reached by increasing the liquid resistance R_L: the exponential part is dominant and makes the linear part to disappear. The derivative of Eq. (7) at the time $t = 0$ is computed to get the equation of the approximating straight line, resulting to the initial slope expression of the wave segment function given by the following equation:

$$\left.\frac{dv_u}{dt}\right|_{t=0} = \beta - \frac{2\zeta}{\tau\left(1+e^{-\frac{T}{\tau}}\right)} \qquad (9)$$

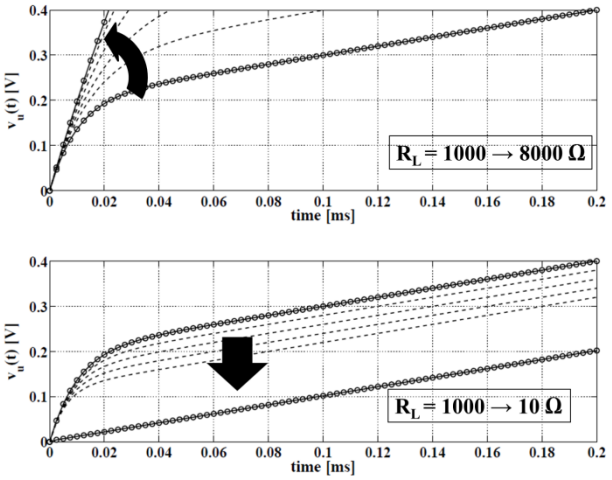

Fig. 6: Increase and decrease effect of the exponential part of the analog voltage illustrating the case $\tau << T$ (top view) and $\tau >> T$ (bottom view).

According to the comparison between τ and T, the quantity $e^{-T/\tau}$ can be approximated to one. The approximating straight voltage equation is thus given by Eq. (10). Replacing β, ζ and τ by their respective electrical component expression, the total sensor capacitance C_L+C_B can be extracted following the input values of C_S and I_0. The parasitic capacitance C_B is calculated according to Eq. (4), the parasitic permittivity ε_B is fixed by the IDE structure board material.

$$v_u(t) = \left(\beta + \frac{\zeta}{\tau}\right)t = I_0\left(\frac{1}{C_S} + \frac{1}{C_L+C_B}\right)t \qquad (10)$$

The second case happens when the linear part of $v_u(t)$ is predominant. The exponential part of the wave segment $v_u(t)$ becomes negligible in comparison with the linear one ($\tau << T$). The bottom curves of Fig. 6 show how the linear part is becoming predominant when the exponential part is going down. The wave segment

equation is written as Eq. (11). This case occurs when the IDE sensor equivalent impedance magnitude is negligible in Eq. (5). The system response is perfectly triangular with a slope equal to the β parameter and therefore inversely proportional to the additional capacitance C_S.

$$v_u(t) = \beta t = \frac{I_0}{C_S} t \qquad (11)$$

The last case for which both parts of $v_u(t)$ are appearing distinctly corresponds to the general form of the segmented voltage $v_u(t)$ and is used to extract the fluid resistance R_L. Focusing on the ζ' parameter, the exponential term $e^{-T/\tau}$ can be approximated to zero with an error of less than 1% when the condition $T > 5\ \tau$ is satisfied. The parameter ζ' is therefore substituted by $2\ \zeta$ as given by Eq. (12), the ζ parameter being directly linked to the fluid resistance R_L.

$$v_u(t) = \beta t + 2\zeta \left(1 - e^{\left(-\frac{t}{\tau}\right)}\right) \qquad (12)$$

IV. SYSTEM DESIGN

The system interface block diagram is given in Fig. 7. The system consists in two opposite current sources that are alternatively enabled and disabled by a digital command $v_d(t)$ which is the system feedback control signal. The swing of the analog wave $v_a(t)$ is limited by the hysteresis of a Schmitt trigger. The system polarity changes each time $v_a(t)$ reaches the upper or the lower limit of the hysteresis voltage.

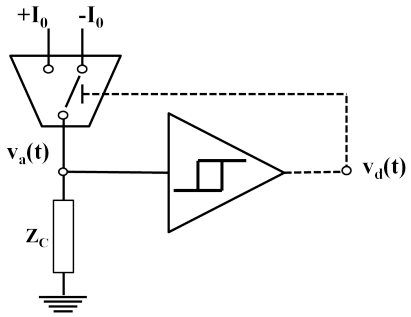

Fig. 7: System block diagram.

The CCO architecture of the closed-loop system generates an oscillating signal and has been designed on CMOS advanced technologies in [10] and in Fig. 8. In the present work, as our goal is to prove an instrumentation concept and not yet to design a CMOS integrated sensor interface, we propose a similar architecture implemented with bipolar transistors to mirror the load current. The MOSFET devices act as switches to invert the circuit polarity. The analog voltage is monitored by a Schmitt NAND gate which yields the feedback digital control to change the current load polarity. A high input impedance analog buffer has been added to avoid deforming the triangular wave due to the relatively low input impedance of the probing equipment.

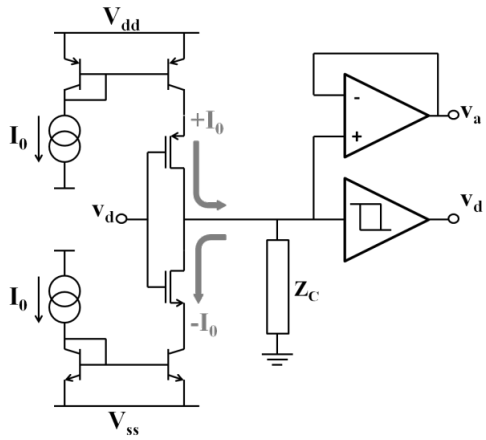

Fig. 8: System circuit architecture.

V. MEASUREMENTS RESULTS

The circuit architecture of Fig. 7 has been implemented on a standard PCB platform (Multi Circuit Boards Ltd.) using discrete components listed in Table 3. The board includes two output connectors used to probe the analog voltage and the digital control signal. The supply voltage of the analog buffer and the Schmitt trigger is set at 5 V. The trigger hysteresis amount is fixed by the supply voltage and is equal to 0.9 V. The serial capacitance C_S value of the system is set to 90 nF to fix an output frequency range starting from 100 Hz to 10 kHz respecting the load current amplitude range of 10 µA to 1 mA. The interdigitated structures are made of gold and directly printed on the circuit board. Although the selection of the PCB technology limits the dimensions of the electrodes, it allows a fast and cheap prototyping.

Table 3: PCB prototype components annotations and models.

Component type	Name
PNP bipolar mirror	BCV62
NPN bipolar mirror	BCV61
CMOS switch	ADG636
Schmitt NAND gate	CD4093
Analog amplifier	AD8661ARZ

The analog voltage measurements have been performed using lumped components of high precision (< 0.1%) that represent the IDE sensor electrical model. The tested components are listed in Table 4; the analog voltage is probed with the *Agilent Infiniium MSO8104A* oscilloscope and plotted in Fig. 9. As the system works in closed-loop, the analog wave oscillates between the two defined hysteresis levels. The values of the lumped elements have been extracted according to Eq. (7). The

measured values given in Table 4 are compared to the calibrated values of the lumped components. We see that the largest error is observed for the C_L capacitance extraction.

Table 4:Tested lumped components calibrated and extracted values according to Eq. (7).

Signal	R_L [Ω]	C_L [nF]	C_S [nF]	
$v_a(t)_{11}$	1100	10	90	cal.
	1140	10.5	86.5	meas.
	3.6%	5%	3.9%	err.
$v_a(t)_{12}$	1600	10	90	cal.
	1670	10.7	86.7	meas.
	4.2%	7%	3.7%	err.
$v_a(t)_{13,21}$	2100	10	90	cal.
	2049	10.7	87.2	meas.
	2.4%	7%	3.1%	err.
$v_a(t)_{22}$	2100	25	90	cal.
	2152	24.7	87.9	meas.
	2.4%	1.2%	2.3%	err.
$v_a(t)_{23}$	2100	40	90	cal.
	2187	38.7	88.7	meas.
	4%	3.2%	1.4%	err.

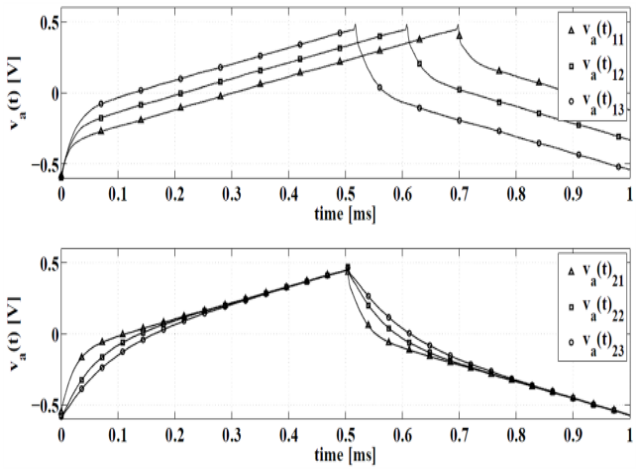

Fig. 9: Analog voltage versus time for different values of R_L (top view) and C_L (bottom view), the legend details are reported in Table 4.

NaCl and KCl test solutions have been prepared and calibrated using an industrial conductimeter (EUTECH CON 270, 1% full scale accuracy). The IDE sensor dimensions reported in Table 5 are chosen according to the theoretical prediction of the solutions conductivities using Eq. (13) in order to set a total range of liquid resistance R_L measurable by the system; c_{XCl} being the saline concentration (mol^{-1}) and the molar conductivities being given in Table 6.

$$\sigma_L = c_{NaCl|KCl}\left(\lambda_{Na^+|K^+} + \lambda_{Cl^-}\right) \qquad (13)$$

The conductivities are then extracted using Eq. (4), the cell constant links the conductivity to the measured liquid resistance. The value of the cell constant gives also the IDE capacitance, which is about 50 pF for water ($\varepsilon_L = 80$). This value being out of the PCB system capacitance detection range, an additional capacitance of 5 nF has been thus added in parallel with the IDE sensor. This added capacitance does not modify the performance of the system, the sensitivity remains identical taking into account this value in the processed data.

Table 5: IDE structure parameters for saline solutions tests.

Parameter	Value	Units
W_f	500	[µm]
W_s	500	[µm]
N_f	20	[-]
L_f	11.5	[mm]
c_{kL}	7.5	[m^{-1}]
c_{kB}	7.5	[m^{-1}]
C_B	3.07	[pF]

Table 6: Ionic molar conductivities.

Ion type	λ [$mS.m^2.mol^{-1}$]
Na^+	5.01
K^+	7.35
Cl^-	7.63

The results (Figs. 10 and 11) show the liquid conductance extracted from the system triangular output voltage. The measurements have been repeated ten times. The *x*-axis scale is the electrolyte salt concentration measured by the industrial conductimeter and expressed in $mol.l^{-1}$. We observe an excellent linearity and repeatability of the liquid measurements over the input range from 10^{-6} to 10^{-5} mol^{-1}. In case of higher concentrations, not tested presently, a higher electrolyte concentration means that the liquid resistance is smaller and therefore more difficult to extract, thus the net effect will result in a higher spread.

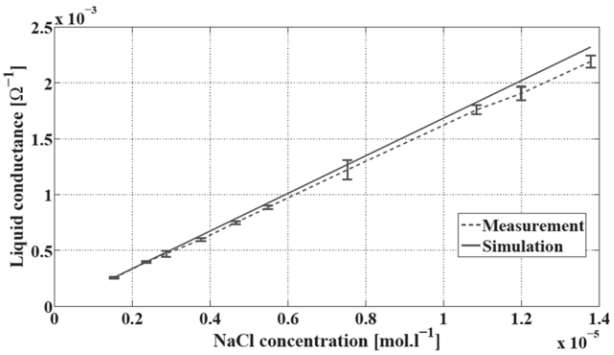

Fig. 10: Experimental (with standard deviation) and theoretical evolution of the NaCl electrolyte conductance vs. salt concentration.

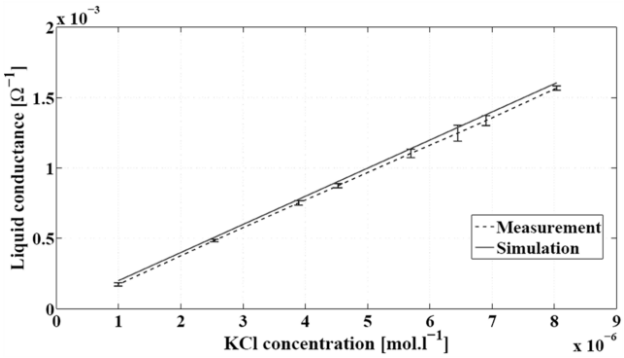

Fig. 11: Experimental (with standard deviation) and theoretical evolution of the KCl electrolyte conductance vs. salt concentration.

VI. DISCUSSION

In every system implementation, the circuit elements are non-ideal and limit the system performances. To extent the measurement range, the probed wave has to be modeled at its best. Any parasitic on the analog output voltage must be identified and avoided. Three main parasitics are presently seen to deteriorate the measurement: 1) the parasitic capacitances of the discrete components, lowering the sensitivity, 2) the circuit bandwidth limited by the Schmitt trigger switching times (~600 ns here), we limited the working frequency under 50 kHz as beyond this frequency the quality of the analog output voltage of our prototype was too much deteriorated, and 3) the performance of the current copy performed by the bipolar transistors, affected by the Early effect and the mismatch between the transistors.

A CMOS design can reduce the parasitics and improve the quality of the current copy since the gate current of MOS devices is negligible in comparison with the base current of bipolar devices. In addition, the silicon integration of the circuit brings a much better matching of the mirror than discrete implementation and lower power.

VII. CONCLUSIONS

A modified triangular waveform voltage detection technique has been demonstrated to sense the *R-C* impedance model of salted liquids. The theoretical result of wave segmentation includes in one compact and simple expression all the information that has to be extracted from an *R-C* parallel dipole of an interdigitated electrodes sensor. The implementation of a closed-loop self-oscillating circuit interface makes the system autonomous and compact. Measurements on saline concentration have been obtained with high accuracy in the 10^{-6} to 10^{-5} mol^{-1} input range. A CMOS integration of the whole system would be the best solution to considerably attenuate the parasitic effects of the devices, to extend the circuit bandwidth and also to reduce the system power consumption.

ACKNOWLEDGMENT

The authors would like to thank the Service Public de Wallonie (Belgium) for funding this research work via the *Skywin HM+* project. They also thank the technical staff of the WELCOME characterization platform.

REFERENCES

[1] V.F. Lvovich, C.C. Liu, Matthew F. Smiechowski, ”Optimization and fabrication of planar interdigitated impedance sensors for highly resistive non-aqueous industrial fluids”, Sensors and Actuators B, vol. 119, pp.490-496, 2006.

[2] Roberto de la Rica, César Fernandez-Sànchez, Antonio Baldi, ”Polysilicon interdigitated electrodes as impedimetric sensors”, Electrochemistry Communications, vol. 8, pp. 1239-1244, 2006.

[3] W. Olthuis, A.J. Sprenkels, J.G. Bomer, P. Bergveld, ”Planar interdigitated electrolyte-conductivity sensors on an insulating substrate covered with Ta_2O_5”, Sensors and Actuators B, vol. 43, pp. 211-216, 1997.

[4] J. Wu, J. P. W. Stark, ”A low-cost approach for measuring electrical conductivity and relative permittivity of liquids by triangular waveform voltage at low frequencies”, Measurement Science and Technology, vol. 16, pp. 1234-1240, 2005.

[5] K-H. Lee, J-O. Lee, M-J. Sohn, B. Lee, S-H. Choi, S. K. Kim, J-B. Yoon, G-H. Cho, ”One-chip electronic detection of DNA hybridation using precision impedance-based CMOS array sensor”, Biosensors and Bioelectronics, vol. 26, pp. 1373-1379, 2010.

[6] J. Lario-Garcìa, R. Pallas-Areny, ”Constant-phase element identification in conductivity sensors using a single square wave”, Sensors and Actuators A, vol. 132, pp. 122-128, 2006.

[7] N. André, S. Druart, P. Dupuis, B. Rue, P. Gérard, D. Flandre, J.P. Raskin, L.A. Francis, ”Dew-Based Wireless Mini Module for Respiratory Rate Monitoring”, IEEE Sensors Journal, vol. 12, pp. 699-706, 2012.

[8] K. Bohinc, V. Kralj-Iglic, A. Iglic, "Thickness of electrical double layer. Effect of ion size", Electrochimica Acta, vol. 46, pp.3033-3040, 2001.

[9] P. Van Gerwen, W. Laureyn, W. Laureys, G. Huyberechts, M. Op De Beeck, K. Baert, J. Suls, W. Sansen, P. Jacobs, L. Hermans, R. Mertens, ”Nanoscaled interdigitated electrode arrays for biochemical sensors”, Sensors and Actuators B, vol. 49, pp. 73-80, 1998.

[10] C. Azcona, B. Calvo, N. Medrano, S. Celma, M. R. Valero, ”A CMOS Micropower Voltage-to-Frequency Converter for Portable Applications”, Ph.D. Research in Microelectronics and Electronics (PRIME), 2011 7th Conference on, vol. 26, pp. 141-144, 2011.